Oil & Gas Science and Technology – Rev. IFP Energies nouvelles **75**, 83 (2020)

https://doi.org/10.2516/ogst/2020075

Available online at:
ogst.ifpenergiesnouvelles.fr

REGULAR ARTICLE OPEN ACCESS

Laboratory investigation of co-precipitation of $CaCO_3/BaCO_3$ mineral scale solids at oilfield operating conditions: Impact of brine chemistry

Zhang Zhang[1], Amy T. Kan[2], Mason B. Tomson[2], and Ping Zhang[3,*]

[1] Arcadis U.S. Inc., San Francisco, CA 94104, USA
[2] Department of Civil and Environmental Engineering, Rice University, Houston, Texas 77005, USA
[3] Department of Civil and Environmental Engineering, Faculty of Science and Technology, University of Macau, Taipa, Macau S.A.R

Received: 29 June 2020 / Accepted: 14 September 2020

Abstract. Oilfield mineral scale deposition can become severe flow assurance challenge especially for offshore deepwater productions. Hazards arising from scale formation and subsequent deposition include production system throughput reduction and eventually blockage. Among various types of scales, carbonates are among the most frequently observed scales in oilfield operations. Similar to many natural and industrial processes, co-precipitation of multiple scales can commonly be observed in oilfield operations. Although extensive research efforts have been made in the domain of understanding the thermodynamics of scale formation, there are limited studies to investigate the kinetic aspect of scale formation, particularly the kinetics of co-precipitation of multiple scales. In this study, the kinetic characteristics of $CaCO_3/BaCO_3$ co-precipitation have been experimentally investigated at representative oilfield conditions of 80 °C and 1 M NaCl condition. The focus was given to the investigation of the impact of different brine chemistry conditions such as mineral saturation level and Ca to Ba molar ratio. The experimental results suggest that $CaCO_3$ saturation level, substrate material and molar ratio can impact the nature and morphology of the carbonate scales formed. An elevation of $CaCO_3$ saturation index from 0.6 to 2 will change the formed carbonate solids from calcite to aragonite. In addition, at a Ca:Ba molar ratio of 1:15 with an excessive aqueous Ba species available, Ba species can partition into $CaCO_3$ crystal lattice to distort $CaCO_3$ lattice, resulting in almost 2-fold increase in aqueous Ca concentration. The results and conclusions from this study have the potential to benefit oilfield scale control strategy development, particularly the one related to carbonate scale formation control.

Abbreviations

EDXS	Energy-Dispersive X-Ray Spectrometer
ESD	Electronic Supporting Data
ICP-MS	Inductively Coupled Plasma-Mass Spectrometry
ICP-OES	Inductively Coupled Plasma-Optical Emission Spectrometer
MR	Molar Ratio
SEM	Scanning Electronic Microscopy
SI	Saturation Index
SSP	ScaleSoftPitzer

1 Introduction

Flow assurance is a subject within the petroleum industry to ensure hydrocarbon flow from subsurface reservoir to the point of sale in a safe and economical manner (Gudmundsson, 2017). Other than multiphase flow simulation, flow assurance engineers deal with managing the formation and subsequent precipitation of unwanted solids from either hydrocarbon phase or water phase. Depending on the nature of these oilfield precipitated solids, some of the common oilfield flow assurance challenges include mineral scale precipitation, asphaltene precipitation, hydrate blockage, to name a few. Properly handling these flow assurance challenges become especially critical for offshore deepwater operations where the operating conditions of high reservoir pressure, low seawater temperature and high salinity can considerably exacerbate the flow assurance issues (Gao *et al.*, 2006; Wang *et al.*, 2018). Laboratory studies and field observations suggest that flow assurance related operational issues can result in a substantially elevated operational risk as well as a significant financial loss (Gao *et al.*, 2006; Mackay *et al.*, 2005; Zhang *et al.*, 2017). Mineral scale (hereafter referred to as "scale") is the hard crystalline inorganic precipitate formed from the

* Corresponding author: pzhang@um.edu.mo

aqueous phase. Scale formation is a ubiquitous phenomenon in nature and in daily life. However, massive scale formation and subsequent precipitation can lead to throughput reduction and eventually pipe/conduit blockage in various industrial processes (Bukuaghangin *et al.*, 2016; Ghaderi *et al.*, 2009; Jordan *et al.*, 2012; Kan and Tomson, 2012; Lecerf *et al.*, 2005; Rostami *et al.*, 2019; Vazquez *et al.*, 2016; Zhang *et al.*, 2018b). Scale associated operational issues are particularly challenging in oilfield operations and especially in deepwater productions (Fink, 2011). Scale particles can form in the pore space of wellbore formation, leading to a severe formation damage (Moghadasi *et al.*, 2019a, b). The most commonly observed oilfield scales include carbonate scales, particularly calcium carbonate ($CaCO_3$). The formation of $CaCO_3$ is mainly driven by pressure reduction from reservoir to different upstream locations of the production system (Frenier and Ziauddin, 2008; Kan and Tomson, 2012; Kan *et al.*, 2019). The reduction in pressure will result in evolution of CO_2 gas from aqueous solution, giving rise to a higher solution pH and subsequent dissociation of bicarbonate into carbonate. The combination of Ca ion, which is abundant in oilfield produced water, with the formed carbonate species can lead to $CaCO_3$ precipitation. For a typical oilfield, the water cut will normally increase considerably towards the end of the field life (Fink, 2011). This suggests that the amount of scale formation can markedly rise together with produced water. Other than $CaCO_3$ scale, other types of carbonate scales are also frequently observed in oilfield operations, such as barium carbonate ($BaCO_3$). Barium species is commonly present in oilfield produced water with an aqueous concentration ranging from less than 0.1 mg L^{-1} to over 2000 mg L^{-1} (Neff and Sauer, 1995).

It has been discussed in a number of recent studies that thermodynamics and kinetics are two key aspects of the scale deposition process (Bukuaghangin *et al.*, 2016; Sanni *et al.*, 2017; Zhang *et al.*, 2018a, 2019). Thermodynamic studies aim at understanding the extent of scale saturation and the amount of scale solid precipitated. The most critical notion in the thermodynamic study is the Saturation Index (SI) which indicates the level of aqueous solution superstation with respect to the solid of concern (Frenier and Ziauddin, 2008; Kan and Tomson, 2012; Kan *et al.*, 2019). SI is calculated as the base 10 logarithm of the ratio of ion activity product with solubility product (Pitzer, 1991). If a SI value is higher than zero, this suggests that the solution is supersaturated with the solid and scale deposition is expected. If SI is lower than zero, scale threat will not be anticipated. As the chemical driving force, SI can be impacted by various factors, such as, pressure, temperature and water chemistry. Extensive studies have been carried out for the purpose of calculating SI at different operating conditions. Particularly, efforts have been made in the calculation of activity coefficient as a function of system conditions and brine chemistry (Kan and Tomson, 2012; Kan *et al.*, 2019; Pitzer, 1991; Zuber *et al.*, 2013). A number of commercial software packages are available for this purpose.

However, as elaborated by a number of authors that these thermodynamic calculations have no consideration of scale deposition kinetics and thus are not able to predict the kinetics of scale deposition, *i.e.*, how long it will take for a supersaturated solution to form scale deposits (Mackay, 2003; Sanni *et al.*, 2017; Yuan, 2010; Zhang *et al.*, 2018a). As for various industrial processes, such as oilfield productions, the knowledge of scale deposition kinetics can be equally important as scale deposition thermodynamics, if not more so. It is often observed that scale deposition kinetics for a mildly supersaturated brine can be kinetically slow and it can take a longer time for the brine solution to flow out of the oilfield production system than the time duration required for scale deposition. As such, the field scale management strategy can be completely different for scenarios with a similar SI value but vastly different deposition kinetics. Although supersaturation or SI is perhaps the most significant impact factor on scale deposition kinetics, a number of other physicochemical parameters can have a significant influence on scale deposition kinetics. Some of these factors include flow rate, hydrodynamic condition, surface properties, to name a few. Thus, although thermodynamic studies have well established the theoretical basis of scale depositions, there are limited studies in the domain of scale deposition kinetics due to its complicated nature (Zhang *et al.*, 2018a, 2019). Recently, a few studies have elaborated several laboratory approaches to evaluate the kinetic process of scale deposition experimentally (Bukuaghangin *et al.*, 2016; Sanni *et al.*, 2017; Zhang *et al.*, 2018a, 2019). These experimental approaches include plug-flow type tubing device, once-through flow visualization equipment and rotating cylinder setup. These studies suggest that scale deposition process involves a number of consecutive stages with different kinetic patterns. Moreover, water chemistry and system conditions such as surface adhesion and heterogeneous surface crystallization can play an influential role in impacting scale deposition kinetics. As discussed previously, most of the precipitated scale solids in nature and in industry are actually mixtures of multiple types of scales, owing to different formation pathways, such as isomorphous lattice replacement (Mullin, 2001; Stumm and Morgan, 1996). This co-precipitation phenomenon suggests that conclusions obtained from studying individual mineral scale might not be suitable for interpreting systems with multiple scales and the presence of other scales can profoundly impact scale deposition kinetics. In a previous study, co-precipitation kinetics of barium sulfate and strontium sulfate has been experimentally investigated at represented oilfield conditions (Zhang *et al.*, 2019). A cationic solution containing Ba and Sr species was mixed with another anionic solution containing SO_4 species. A key conclusion from the study was that the presence of Ba species can expedite the precipitation kinetics of $SrSO_4$ scale solid. It was speculated that the formation of $BaSO_4$ solids served as the nuclei to promote $SrSO_4$ solid precipitation. Additional study results are available for the system of $CaCO_3$ and $CaSO_4$ (Chong and Sheikholeslami, 2001; Safari and Jamialahmadi, 2014; Zarga *et al.*, 2013). These studies suggest that $CaCO_3$ precipitation process is promoted by the presence of $CaSO_4$ solid which is speculated to reduce $CaCO_3$ solid nucleation energy barrier.

As discussed above, both Ca and Ba species are commonly present in oilfield produced water. Due to pressure reduction during hydrocarbon production process, carbonate solids can be formed as a result of CO_2 evolution and solution pH rise. One can speculate that the presence of Ca species can impact the scale deposition kinetics of $BaCO_3$ and *vice versa*. In this study, the kinetic characteristics of $CaCO_3/BaCO_3$ co-precipitation have been experimentally investigated at representative oilfield conditions. The focus was given to the evaluation of the impact of different brine chemistry conditions such as saturation level and Ca to Ba Molar Ratio (MR). The morphology of the formed carbonate scale solids was characterized by electron microscope. Both beaker test setup and flow-through tube reactor were adopted to understand the impact of SI and substrate material at different Ca to Ba MRs. To the best of the authors' knowledge, this paper is the first to report the precipitation kinetics of $CaCO_3/BaCO_3$ mineral scales at representative oilfield conditions in a systematic manner. The results and conclusions from this study have the potential to benefit oilfield scale control strategy development, particularly the one to control carbonate scale formation. These benefits include better understanding of the carbonate scale threats at complicated water chemistry conditions and elimination of possible underestimation of scale threat due to carbonate co-precipitation.

2 Materials and methods

2.1 Chemicals

Solids of sodium chloride (NaCl), calcium chloride ($CaCl_2$), barium chloride ($BaCl_2$), and sodium bicarbonate ($NaHCO_3$) were reagent grade and purchased from *Fisher Scientific*. Hydrogen chloride (HCl) and sodium hydroxide (NaOH) were reagent grade and purchased from *Sigma-Aldrich*. Deionized water was prepared by reverse osmosis and ion exchange water purification processes.

2.2 $CaCO_3/BaCO_3$ co-precipitation in beaker test

To evaluate the crystal morphology of co-precipitated $CaCO_3/BaCO_3$ mineral solids, a beaker test was carried out at an ambient condition of 23 °C and 1 bar inside a glass beaker. To begin with, stock solutions of $CaCl_2$, $BaCl_2$ and $NaHCO_3$ were prepared by adding the respective solids into 1 M NaCl brines. Next, the stock solutions of $CaCl_2$ and $BaCl_2$ were mixed to prepare a Ca–Ba mixture brine solution with a Ca to Ba molar ratio (Ca:Ba MR) of 1:15. These prepared brine solutions were all set to the same pH value of 8.7 by adding NaOH or HCl to minimize CO_2 exchange. Precipitation of carbonate scale solids was achieved by adding $NaHCO_3$ brine solution into the $CaCl_2$, $BaCl_2$ or Ca–Ba mixture brine solution under constant stirring inside a glass beaker. A magnetic stirrer was placed inside the glass beaker prior to solution addition to facilitate solution mixing. The $NaHCO_3$ brine solution was delivered by a plastic syringe propelled by a syringe pump and the solution addition was normally completed within 30 s. Table 1 summarizes the experimental conditions for the beaker tests (Exp. Beaker-1 to Beaker-3). The obtained precipitated mineral solids from the beaker tests were collected for instrumental analysis and characterization.

2.3 $CaCO_3$ surface coating of plug-flow tube reactor

Similar to the previously reported studies (Zhang *et al.*, 2019), a plug-flow type tube reactor was adopted in this study to evaluate carbonate scale deposition behavior. The dimension of the tube reactor is 12.7 cm by length and 0.46 cm by inner diameter. The schematic of the reactor setup is shown in the ESD Section S1. The photo images and pre-treatment of tube reactors are shown in the ESD Section S2 & S3. Two peristaltic pumps (Biotech P-500, Pharmacia) were employed for brine solution delivery. Coating of $CaCO_3$ solid on the interior surface of the tube reactor was realized by delivering a $CaCl_2$ brine solution and another $NaHCO_3$ brine solution simultaneously into the tube reactor placed inside a water bath of 80 °C at 1 bar. The composition of the combined brine flowing through the tube reactor is shown in Exp. Coating-1 in Table 1. Brine solution delivery was achieved by pumping the brine solution at a flow rate of 100 mL h^{-1} or a linear flow velocity of ca 0.17 cm s^{-1}. It normally took 30–40 h to complete the brine delivery for tube reactor surface coating. To have a better understanding of the $CaCO_3$ coating, a number of impact factors were evaluated for their roles in the coating process, including reactor materials, saturation index and surface roughness of tube reactor. Two types of tube reactor materials were adopted in this study including seamless 1010 mild steel (*Grainger*, Houston TX) and seamless 316 stainless steel (*Grainger*, Houston, TX). Brine solution in Exp. Coating-1 was employed to evaluate the impact of tube reactor materials. The impact of saturation index was investigated by pumping through the stainless steel tube reactor with another brine solution of a different composition (Exp. Coating-2 in Tab. 1). The impact of surface roughness was studied by use of stainless steel tube reactors and brine solution in Exp. Coating-1 in Table 1. Two stainless steel tube reactors of different surface roughness were adopted and photo images of these two stainless steel reactors are shown in the ESD Section S4.

2.4 Co-precipitation of carbonate scales on the surface of tube reactors

Following the surface coating of $CaCO_3$ on the interior surface of stainless steel tube reactor, the coated reactor was utilized to carry out $CaCO_3/BaCO_3$ co-precipitation experiments. One pump delivered the cationic solution containing Ca or Ca–Ba, and another pump for $NaHCO_3$ solution delivery. These experiments were carried out at 80 °C and 1 bar condition. The brine solutions flowing through the tube reactor all contained 1 M NaCl with a pH of 8.7 as shown in Exp. Precipitation-1 to Precipitation-4 in Table 2. Two different flow rates of 100 mL h^{-1} and 4 mL h^{-1} were tested. The effluent solutions from the tube reactor were collected to measure Ca and Ba

Table 1. Brine compositions and experimental conditions for beaker tests and $CaCO_3$ coating on the interior surface of tube reactor at the condition of 1 bar and 1 M NaCl.

Exp. #	Ca^{2+} mg L^{-1}	Ba^{2+} mg L^{-1}	HCO_3^- mg L^{-1}	Ca:Ba Molar ratio	$CaCO_3$ SI[a]	$BaCO_3$ SI[a]	pH[b]	Testing temp (°C)
Beaker-1	91.8	0	279.5	NA	1	NA	8.7	23
Beaker-2	0	350.0	277.5	NA	NA	1	8.7	23
Beaker-3	23.7	1212.9	533.2	1:15	1	2	8.7	23
Coating-1	40.5	0	122.5	NA	0.6	NA	8.7	80
Coating-2	80.6	0	245.8	NA	2	NA	8.7	80

[a] The reported SI values are calculated at respective experimental conditions (23 or 80 °C) 1 bar.
[b] pH values were measured at an ambient condition of 23 °C and 1 bar.

Table 2. Brine compositions and experimental conditions for co-precipitation of $CaCO_3/BaCO_3$ on the surface of tube reactor at the condition of 80 °C, 1 bar and 1 M NaCl.

Exp. #	Ca^{2+} mg L^{-1}	Ba^{2+} mg L^{-1}	HCO_3^- mg L^{-1}	Ca:Ba Molar ratio	$CaCO_3$ SI[a]	$BaCO_3$ SI[a]	pH[b]	Flow rate mL h^{-1}
Precipitation-1	78.2	0	238.2	NA	1	NA	8.7	100
Precipitation-2	78.2	0	238.2	NA	1	NA	8.7	4
Precipitation-3	78.3	240.5	238.2	1:1	1	1	8.7	4
Precipitation-4	81.1	4221.8	245.6	1:15	1	2	8.7	4

[a] The reported SI values are calculated at the experimental conditions of 80 °C and 1 bar.
[b] pH values were measured at an ambient condition of 23 °C and 1 bar.

concentrations. Instrumental analyses and characterization were performed to study the deposited scale solids.

2.5 Analytical methods

Concentrations of cationic species of Ca and Ba were measured by inductively coupled plasma-optical emission spectrometer (ICP-OES) (Optima 4300, *PerkinElmer*). Inductively coupled plasma-mass spectrometry (ICP-MS, *PerkinElmer*) was adopted for Mn and Cr concentration measurement. Surface morphologies of the deposited carbonate solids were characterized by Scanning Electronic Microscopy (SEM) (*FEI Quanta 400*, Hillsboro, Oregon). The SEM instrument was equipped with an Energy-Dispersive X-Ray Spectrometer (EDXS) for elemental analysis. Saturation index of the carbonate solids was calculated using ScaleSoftPitzer software version SSP2018 (hereafter abbreviated as SSP) (Kan and Tomson, 2012; Kan *et al.*, 2019). Fundamentals of the saturation index calculation are shown in ESD Section S5.

3 Results and discussion

3.1 $CaCO_3/BaCO_3$ co-precipitation in beaker test

The beaker test was designed to evaluate the crystal morphology of the precipitated $CaCO_3/BaCO_3$ mineral scale solids and also to provide the technical insights for evaluation of experimental results obtained from the tube reactor below. In the beaker tests, three different scenarios with respect to different Ca and Ba concentrations were tested at otherwise the same experimental condition to understand the brine composition impact on the obtained mineral solids (Exp. Beaker-1 to Beaker-3 in Tab. 1). In the presence of scaling ions (Ca and/or Ba), the solutions were calculated to be supersaturated with the corresponding mineral solids ($CaCO_3$ and/or $BaCO_3$). SEM characterization was conducted to examine the carbonate solids obtained from Exp. Beaker-1 to Beaker-3. Figure 1 shows that rhombohedral $CaCO_3$ and orthorhombic $BaCO_3$ solids can be formed in the absence of foreign species (Exp. Beaker-1 and Beaker-2), as shown in Figures 1a and 1b. When Ca and Ba co-exist with a MR of 1:15 (Exp. Beaker-3), it seems that $BaCO_3$ solid formed on the surface of $CaCO_3$ solid. In other words, $CaCO_3$ solid seems to form prior to $BaCO_3$ solid and can serve as a medium for $BaCO_3$ solid nucleation (Fig. 1c). In addition, it is obvious that $CaCO_3$ and $BaCO_3$ precipitated separately instead of inclusively. The difficulty for Ba species to partition into the crystal lattice of $CaCO_3$ can be expected due to the difference in the ion radius. It is reported that Ba^{2+} species is about 50% larger than that of Ca^{2+} species (Wang and Xu, 2001). Although the integration of Ba^{2+} into $CaCO_3$ crystal would be difficult, a number of studies show that a fraction of the aqueous Ba species can actually partition into the $CaCO_3$ crystals (Mavromatis *et al.*, 2018; Tesoriero and Pankow, 1996; Yoshida *et al.*, 2008). These research

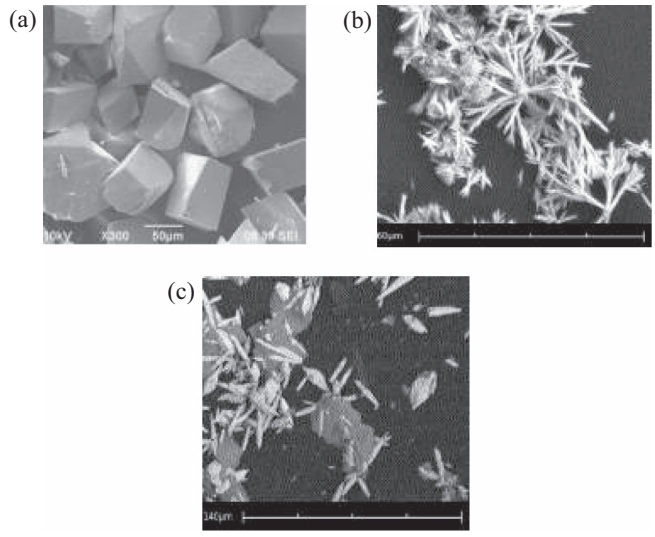

Fig. 1. SEM microimages of the mineral solids obtained from (a) Exp. Beaker-1; (b) Exp. Beaker-2; and (c) Exp. Beaker-3.

findings and the comparison with the finding of this study will be discussed below.

3.2 $CaCO_3$ surface coating of plug-flow tube reactor

Considering the merits of plug-flow tube reactor in investigating solid precipitation phenomenon (Zhang *et al.*, 2018a), this study adopted a similar device of a plug-flow type tube reactor to study the precipitation of carbonate solids. As reported in the previous study, coating a layer of $CaCO_3$ on the interior surface of the tube reactor can facilitate the subsequent deposition of $CaCO_3$ solids and effectively retain phosphonate scale inhibitors (Zhang *et al.*, 2018a). Thus, in this study, the first experiment after the completion of the pre-treatment of tube reactor was to coat the inner surface of the tube reactor with a layer of $CaCO_3$ solids by flowing a bring solution supersaturated with $CaCO_3$. Surface coating experiment was performed at 80 °C and 1 M NaCl solution ionic strength condition to simulate common oilfield operational condition. The impact of reactor materials, brine solution Saturation Index (SI) and surface roughness was evaluated experimentally. Both mild steel and stainless steel were adopted in this study as tube reactor materials. $CaCO_3$ surface coating experiment was carried out following the experimental conditions detailed in Exp. Coating-1 in Table 1. It shows that corrosion-induced elements, such as Fe, Mn and Cr can be detected by ICP-OES and ICP-MS in the effluent solutions from mild steel reactor; while these elements were non-existent in the effluent solutions from stainless steel reactor. Normally, mild steel contains 0.05–0.25% carbon, leading to a poor corrosion resistance compared with stainless steel (Islam *et al.*, 2018; Saleh *et al.*, 2019). Clearly, the tested mild steel can be readily corroded by flowing the brine solution in Exp. Coating-1 during the surface coating experiment. Figure 2 shows that the effluent Fe concentration is in the range of 0 to 12 mg L^{-1}; while Mn and Cr concentrations are in the level of μg L^{-1}. Moreover, both

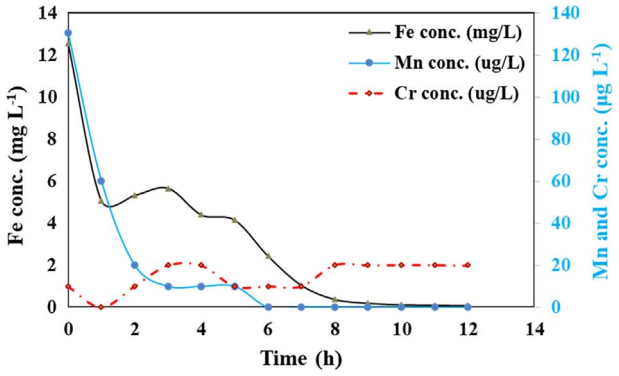

Fig. 2. Effluent species concentrations during coating experiment by use of a mild steel tube reactor.

Fe and Mn concentrations drop substantially following the onset of the coating experiment. Cr concentration, on the other hand, gradually increased to the level of 2 μg L^{-1} and maintained at this level. From the perspective of surface morphology, due to surface corrosion phenomenon, the formed $CaCO_3$ layer on the inner surface of mild steel reactor is uneven with a porous structure, as shown in the SEM image (Fig. 3a). The continuous reduction of Fe and Mn concentration during the course of surface coating experiment can be explained by the formation of an iron (hydro)oxide thin film on the reactor surface inhibiting subsequent surface corrosion. Another explanation of this phenomenon is the integration of these two elements into $CaCO_3$ lattice. This argument can be verified by the EDXS analysis of the co-precipitated mineral crystals as shown in Figure 3b. EDXS characterization suggests that the presence of Fe in the $CaCO_3$ crystals can be verified and Fe element accounts for as much as 16% of total elemental accounts. However, Mn or Cr element cannot be detected *via* EDXS, probably due to its limited mass in the sample. Thus, because of the inclusion of foreign element (mainly Fe in this case), the formed $CaCO_3$ layer on the surface of the mild steel tube reactor is uneven and porous. Based on the above discussion, it is more desirable to employ stainless steel as the tube reactor material due to the consideration of the adverse impact of mild steel material corrosion.

Another factor impacting the $CaCO_3$ surface coating process is the solution SI with respect to $CaCO_3$, abbreviated as SI($CaCO_3$). In this study, two SI($CaCO_3$) values of 0.6 and 2 were tested, *i.e.*, Exp. Coating-1 and Coating-2. A higher SI($CaCO_3$) suggests of a higher scaling tendency. SEM characterization (Fig. 4) suggests that at a higher SI of 2, the dominate crystal form of the precipitated $CaCO_3$ solid is orthorhombic aragonite with a minor fraction of rhombohedral calcite. At a reduced SI of 0.6, the majority of the formed crystals are rhombohedral calcite. In a previous study, it has been shown that an expedited scale precipitation and a higher concentration of carbonate will favor the formation of aragonite over calcite (Given and Wilkinson, 1985; Zhang *et al.*, 2018a). In this study, the experiment with SI($CaCO_3$) of 2 (Exp. Coating-2) has a higher bicarbonate concentration, indicative of a higher concentration of carbonate species considering the same

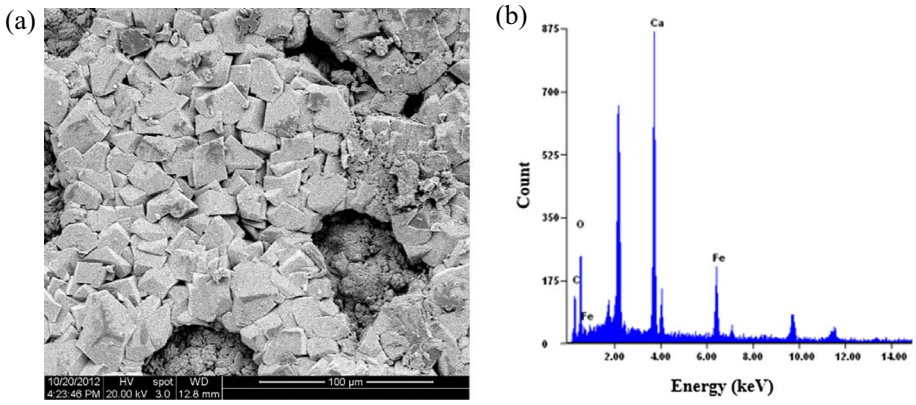

Fig. 3. (a) SEM and (b) EDXS characterization of the obtained carbonate solids from the surface of mild steel tube reactor.

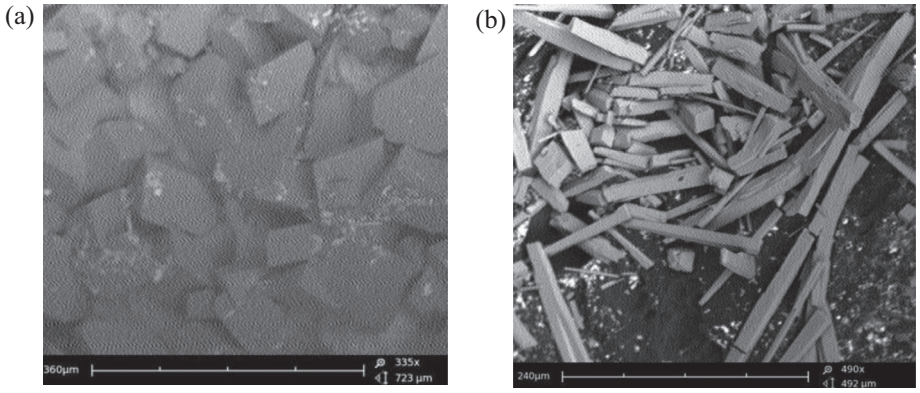

Fig. 4. SEM microimages of the precipitated carbonate solids from the surface of stainless steel tube reactor at (a) SI($CaCO_3$) = 0.6 and (b) SI($CaCO_3$) = 2.

solution pH of 8.7. Thus, the observation in this study is in line with the previously reported $CaCO_3$ morphology study results. Furthermore, this study also evaluates the impact of reactor material surface roughness on $CaCO_3$ surface coating. Two different stainless steel materials with different surface roughness were adopted in this study. Normally, reduction in surface roughness can lead to an enhanced corrosion resistance and a reduced friction with a more lustrous appearance. This study suggests that surface roughness can considerably influence the formed $CaCO_3$ solid on the stainless steel surface. $CaCO_3$ crystals formed on a smoother (mirror-like) surface can be easily removed or fall off from the surface. On the other hand, $CaCO_3$ formed on the surface with a higher roughness seems to be firmly attached to the surface (see ESD Section S6 for details). Based on the definition of surface roughness, an elevated surface roughness can increase the total surface area, providing more nucleation sites for precipitation. A previous experimental study on the fouling behavior of $CaCO_3$ suggests that an increase in surface roughness can lead to an increase in the attachment of the $CaCO_3$ solid and thermal resistance (Lei *et al.*, 2011).

3.3 Co-precipitation of carbonate scales on the surface of tube reactors

Once the interior surface of tube reactor was coated with a layer of $CaCO_3$, co-precipitation of $CaCO_3/BaCO_3$ experiment was carried out at 80 °C and 1 M NaCl condition. The experimental details are shown in Table 2. For all experiments, the aqueous Ca and bicarbonate concentrations were set at *ca.* 80 mg L^{-1} and 240 mg L^{-1}, respectively. Thus, SI($CaCO_3$) was maintained at 1 for all experiments. Two different Ca:Ba MRs were tested to evaluate the impact of Ba concentration and SI($BaCO_3$). To begin with, the influence of flow rate was examined to understand its impact on carbonate scale deposition inside the tube reactor. In the absence of Ba species, a mixture brine solution supersaturated with $CaCO_3$ was injected into the tube reactor at two different flow rates of 100 and 4 mL h^{-1}, respectively and each experiment was run for 60 min (Exp. Precipitation-1 and -2 in Tab. 2). Figure 5 shows that a decrease in flow rate can lead to a noticeable reduction in the effluent Ca species concentration at the end of the experiment (74 *vs.* 61 mg L^{-1}). The thermodynamic

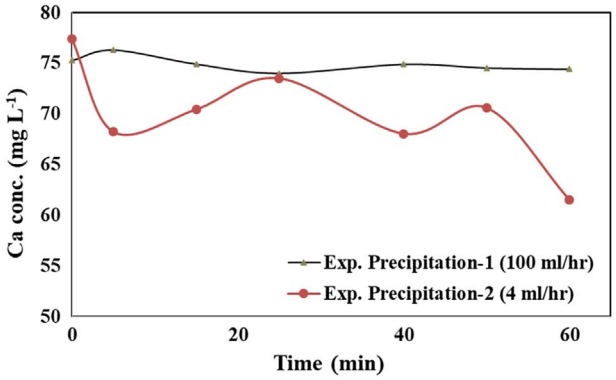

Fig. 5. Effluent Ca concentrations during Exp. Precipitation-1 (100 mL h^{-1} follow rate) and Precipitation-2 (4 mL h^{-1} flow rate).

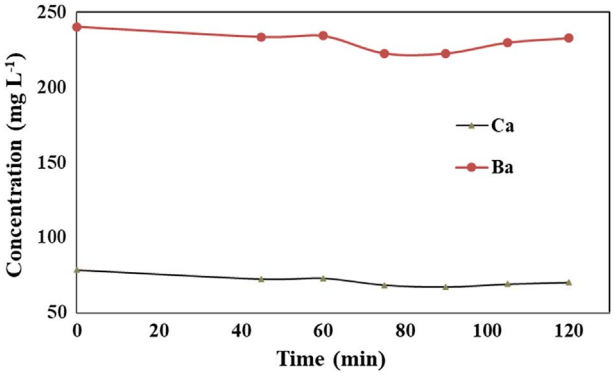

Fig. 6. Effluent Ca and Ba species concentration during Exp. Precipitation-3.

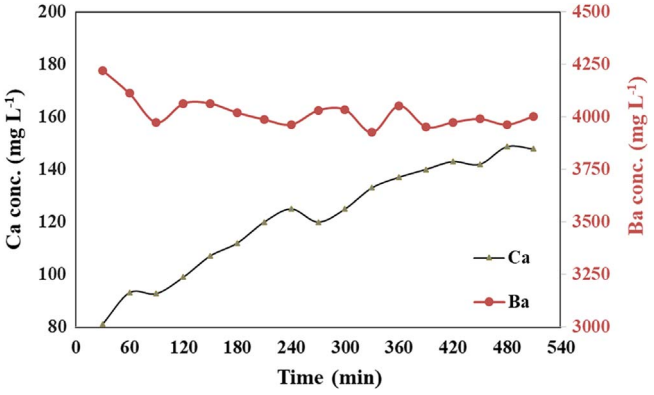

Fig. 7. Effluent Ca and Ba species concentration during Exp. Precipitation-4.

equilibrium concentration of Ca is calculated to be 32.8 mg L^{-1} by use of SSP. Thus, the mass transfer coefficient can be calculated to be 3.5×10^{-6} and 1.4×10^{-5} cm s^{-1}, respectively (see ESD Section S7 for details). In other words, a lower flow rate results in a higher mass transfer, indicative of more $CaCO_3$ precipitating onto reactor surface. This conclusion agrees with the observation reported previously (Zhang *et al.*, 2018a). In this previous study, the impact of flow rate was evaluated while investigating $CaCO_3$ scale deposition kinetics under experimental conditions of various temperature and SI values. It showed that for all experimental conditions studied, a decrease in flow rate will lead to an enhanced $CaCO_3$ deposition.

To evaluate the impact of the presence of Ba species, a mixture brine solution supersaturated with both $CaCO_3$ and $BaCO_3$ was pumped through the $CaCO_3$-coated tube reactor, during which process both $CaCO_3$ and $BaCO_3$ solids would gradually precipitate onto the inner surface of the reactor. Two Ca:Ba MRs are tested including 1:1 and 1:15 at otherwise similar experimental conditions (Exp. Precipitation-3 and -4). Figure 6 shows that when MR is 1:1 (Exp. Precipitation-3), by the end of the scale deposition experiment, both Ba and Ca concentrations slightly reduced where Ca drop from 78 to 70 mg L^{-1} and Ba from 240 to 232 mg L^{-1}. Based on the initial and final Ca and Ba species concentrations, one can calculate the distribution coefficient of Ba into $CaCO_3$ via the following equation:

$$\ln\frac{[\mathrm{Ba}]_f}{[\mathrm{Ba}]_0} = D_{\mathrm{Ba}} \times \ln\frac{[\mathrm{Ca}]_f}{[\mathrm{Ca}]_0},$$

where D_{Ba} is distribution coefficient of Ba into $CaCO_3$. The box bracket represents species concentration. Subscript 0 corresponds to initial stage and subscript f denotes final stage. Considering the species concentrations shown in Figure 6, a D_{Ba} value of *ca.* 0.29 can be calculated assuming homogeneous partitioning of Ba into $CaCO_3$ solid. A number of previous studies also examined the D_{Ba} values by adopting different experimental approaches. It shows that these reported distribution coefficients are generally low, suggesting the difficulty in integrating Ba into $CaCO_3$ lattice. For instance, a number of studies report distribution coefficient values of 0.1 to 1, which are similar to the value obtained in this study (Mavromatis *et al.*, 2018; Tesoriero and Pankow, 1996). D_{Ba} values lower than 0.1 were also reported previously (Yoshida *et al.*, 2008). Mavromatis *et al.* (2018) suggested that ionic radii size plays a dominate role during the metal element incorporation process and solid-solution formation from aqueous solution. In addition, other scholars studied the integration mechanism of Ba^{2+} into $CaCO_3$ and explained the low distribution coefficient value as that little or none of the Ba^{2+} occupy $CaCO_3$ lattice sites. Instead, most of the Ba species were absorbed onto the surface of $CaCO_3$ solids or physically trapped inside the lattice structure as $CaCO_3$ crystal grows (Pingitore, 1987; Yoshida *et al.*, 2008). Furthermore, it was found that although lattice integration of Ba into $CaCO_3$ is challenging, the integrated Ba species would cause significant distortion to the $CaCO_3$ crystal lattice (Pingitore, 1987; Reeder *et al.*, 1999).

In Exp. Precipitation-4, initial Ba concentration was increased to over 4000 mg L^{-1} with the corresponding Ca:Ba MR being changed to 1:15 and the calculated SI ($BaCO_3$) to 2. Figure 7 shows that Ba concentration slightly drop during the course of the experiment from

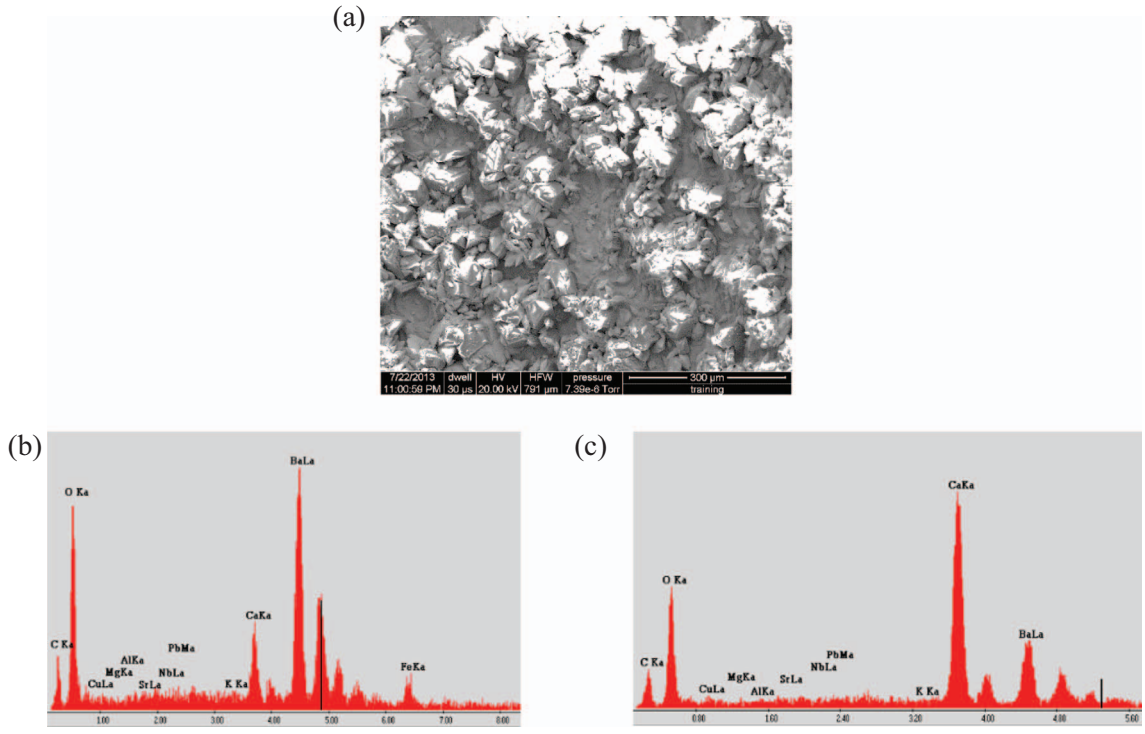

Fig. 8. (a) SEM microimage of the obtained carbonate solids by the end of Exp. Precipitation-4. (b) and (c) EDXS characterizations of the samples at two different sites.

initial concentration of 4200 mg L^{-1} to *ca.* 4000 mg L^{-1}. Interestingly, the aqueous Ca concentration increased from 80 to *ca.* 148 mg L^{-1} by the end of the experiment. Since there is no additional source of Ca other than the flowing fluid and deposited $CaCO_3$ solid, the only plausible reason for the elevated aqueous Ca concentration is the dissolution of the previously precipitated $CaCO_3$ solid from the interior surface of the tube reactor. SEM and EDXS characterization was performed to examine the formed carbonate materials after the completion of Exp. Precipitation-4. SEM image (Fig. 8a) shows that $BaCO_3$ solids formed on the surface of the previously deposited $CaCO_3$ solids. However, the distribution of the precipitated $BaCO_3$ solid is not uniform across the reactor interior surface. This is evidenced by the difference in elemental ratios of Ca and Ba in EDXS results obtained at different sample sites (Figs. 8b and 8c). One possible reason for the increase in Ca concentration during $BaCO_3$ precipitation is ion exchange mechanism. In other words, Ba ions substituted Ca ions in $CaCO_3$ crystal lattice. It can be calculated that the amount of Ca increased is *ca.* 1.67 mmol L^{-1} while the amount of Ba species precipitated is 1.60 mmol L^{-1}. The difference could be a result of analytical error. However, ion exchange mechanism requires the Ba species to completely integrate into the $CaCO_3$ crystal lattice. With a 50% ion radius difference as discussed above, it would be difficult for Ba species to integrate into $CaCO_3$ lattice in a large amount. Another possible explanation is the distortion of $CaCO_3$ crystal lattice by Ba species. A previous study suggests that when Ba species is present in a noticeable amount, it will inhibit $CaCO_3$ precipitation. In addition, Ba species can poison the surface of $CaCO_3$ until the surface is no longer workable (Lorens, 1981; Mavromatis *et al.*, 2018). Thus, a possible explanation for the rise of Ca concentration is the surface poisoning of $CaCO_3$ by Ba species. When Ba is present in a certain quantity in $CaCO_3$ crystal lattice, it could cause significant distortion of the lattice structure of $CaCO_3$. In Exp. Precipitation-4, the high aqueous Ba concentration resulted in a fraction of Ba species being exchanged into $CaCO_3$ crystals, leading to $CaCO_3$ crystal distortion and subsequent $CaCO_3$ dissolution.

4 Conclusion

In this study, experimental efforts have been made to evaluate the co-precipitation process of mixed mineral scales of $CaCO_3/BaCO_3$ at representative oilfield conditions from a kinetics standpoint. The focus was given to evaluate the impact of different brine chemistry conditions on precipitation kinetics, mineral nature and characteristics. Both beaker test setup and flow-through tube reactor were adopted to examine the impact of various physiochemical factors, such as SI, substrate material and MR. Beaker test indicates that $CaCO_3$ solid formed prior to $BaCO_3$ solid and can serve as a medium for $BaCO_3$ solid nucleation. In addition, it is difficult for Ba species to partition into $CaCO_3$ lattice, which is presumed due to Ca/Ba ionic radius difference. A plug-flow tube reactor setup was

employed to study the deposition kinetics of these two carbonate scales at representative oilfield condition of 80 °C and 1 M NaCl. During the interior surface coating of the tube reactor by $CaCO_3$ solid, it shows that substrate material, SI and surface roughness can substantially impact the coating process on reactor surface. Corrosion phenomenon on mild steel surface can result in the presence of *ca.* 16% Fe as total elemental accounts, leading to an uneven and porous surface. The main crystals formed at SI($CaCO_3$) of 2 and 0.6 are orthorhombic aragonite and rhombohedral calcite, respectively. Co-precipitation of mixed $CaCO_3$/$BaCO_3$ scales was carried out using the surface coated tube reactor. The experimental results suggest that a lower flow rate of 4 mL h^{-1} *versus* 100 mL h^{-1} can result in more carbonate scale precipitating onto reactor surface with a four-fold increase in mass transfer coefficient. Furthermore, tube reactor co-precipitation experiments show that although it is difficult for Ba species to integrate into $CaCO_3$ lattice due to Ca/Ba ion radius difference, at an elevated Ca:Ba MR of 1:15 with excessive Ba species available, a fraction of the aqueous Ba species can exchange into $CaCO_3$ crystal lattice, resulting in distortion of $CaCO_3$ and an increase in aqueous Ca concentration from initially 80 mg L^{-1} to eventually 148 mg L^{-1}. The results and conclusions from this study have the potential to benefit oilfield scale control strategy development. These benefits include better understanding of the carbonate scale threats at complicated water chemistry conditions and elimination of possible underestimation of scale threat owning to carbonate co-precipitation.

Supplementary Materials

The supplementary material of this article is available at https://ogst.ifpenergiesnouvelles.fr/10.2516/ogst/2020075/olm

S1. Schematic of the reactor setup

Figure S1. Schematic of the reactor setup.

S2. Steel tube reactors after $CaCO_3$ coating treatment

Figure S2. Tube reactors after $CaCO_3$ coating treatment. The upper reactor is made of mild steel and the bottom one is made of stainless steel.

S3. Tube reactor pre-treatment

S4. Stainless steel tube reactor materials with different roughness

Figure S3. Stainless steel tube reactor materials. (a) High surface roughness (Grainger, Houston, TX); (b) Low surface roughness (Swagelok, Houston, TX).

S5. Saturation index calculation

S6. Impact of surface roughness on $CaCO_3$ surface coating

Figure S4. $CaCO_3$ surface coating using stainless materials of different surface roughness. (a) High surface roughness material; (b) Low surface roughness material. A fraction of the attached $CaCO_3$ was peeled off; (c) SEM image of the edge of $CaCO_3$ on the surface of low roughness material.

S7. Mass transfer coefficient calculation

Acknowledgments. This work was financially supported by The Science and Technology Development Fund, Macao S.A.R. (File no. (0063/2018/A2 and 0141/2019/A3), and *University of Macau* (File no. MYRG2019-00020-FST). The authors appreciate the sponsorship of *Brine Chemistry Consortium companies* of *Rice University*, including *Aegis, Apache, Baker Hughes, Chevron, ConocoPhillips, Clariant, Coastal Chemical, ExxonMobil, Equinor, Flotek Industries, Halliburton, Italmatch, JACAM, Kemira, Kinder Morgan, Oxy, Chemstream, Pioneer, RSI, Saudi Aramco, Schlumberger, Shell, Solugen, SNF, Solvay,* and Total.

References

Bukuaghangin O., Sanni O., Kapur N., Huggan M., Neville A., Charpentier T. (2016) Kinetics study of barium sulphate surface scaling and inhibition with a once-through flow system, *J. Petro. Sci. Eng.* **147**, 699–706.

Chong T.H., Sheikholeslami R. (2001) Thermodynamics and kinetics for mixed calcium carbonate and calcium sulfate precipitation, *Chem. Eng. Sci.* **56**, 5391–5400.

Fink J. (2011) *Petroleum engineer's guide to oil field chemicals and fluids*, Gulf Professional Publishing.

Frenier W.W., Ziauddin M. (2008) *Formation, removal, and inhibition of inorganic scale in the oilfield environment*, Society of Petroleum Engineers.

Gao S., House W., Chapman W.G. (2006) Detecting gas Hydrate behavior in crude oil using NMR, *J. Phys. Chem. B* **110**, 6549–6552.

Ghaderi S.M., Kharrat R., Tahmasebi H.A. (2009) Experimental and theoretical study of calcium sulphate precipitation in porous media using glass micromodel, *Oil Gas Sci. Technol. – Rev. IFP Energies nouvelles* **64**, 4, 489–501.

Given R.K., Wilkinson B.H. (1985) Kinetic control of morphology, composition, and mineralogy of abiotic sedimentary carbonates, *J. Sediment Res.* **55**, 109–119.

Gudmundsson J.S. (2017) *Flow assurance solids in oil and gas production*, CRC Press.

Islam M.M., Pojtanabuntoeng T., Gubner R. (2018) Corrosion of carbon steel under condensing water and monoethylene glycol, *Corros. Sci.* **143**, 10–22.

Jordan M.M., Sorhaug E., Marlow D. (2012) Red *vs.* green scale inhibitors for extending squeeze life – A case study from the North Sea, Norwegian sector – Part II, *SPE Prod. Oper.* **27**, 404–413.

Kan A.T., Dai J., Deng D., Harouaka K., Lu Y.-T., Wang X., Zhao Y., Tomson M.B. (2019) Recent advances in scale prediction: Approach and limitations, *SPE J.* **24**, 2209–2220.

Kan A.T., Tomson M.B. (2012) Scale prediction for oil and gas production, *SPE J.* **17**, 362–378.

Lecerf B., Flamant N., Ziauddin M., Frenier W. (2005) A method for assessing the impact of secondary and tertiary reactions on sandstone acidizing treatments, *Oil Gas Sci. Technol. – Rev. IFP Energies nouvelles* **60**, 2, 319–337.

Lei C., Peng Z., Day T., Yan X., Bai X., Yuan C. (2011) Experimental observation of surface morphology effect on crystallization fouling in plate heat exchangers, *Int. Commun. Heat Mass.* **38**, 25–30.

Lorens R.B. (1981) Sr, Cd, Mn and Co distribution coefficients in calcite as a function of calcite precipitation rate, *Geochim. Cosmochim. Acta.* **45**, 553–561.

Mackay E. (2003) Predicting *in situ* sulphate scale deposition and the impact on produced ion concentrations, *Chem. Eng. Res. Des.* **81**, 326–332.

Mackay E.J., Jordan M.M., Feasey N.D., Shah D.J., Kumar P.S., Ali S.A. (2005) Integrated risk analysis for scale management in deepwater developments, *SPE Prod. Fac.* **20**, 138–154.

Mavromatis V., Goetschl K.E., Grengg C., Konrad F., Purgstaller B., Dietzel M. (2018) Barium partitioning in calcite and aragonite as a function of growth rate, *Geochim. Cosmochim. Acta.* **237**, 65–78.

Moghadasi R., Rostami A., Hemmati-Sarapardeh A., Motie M. (2019a) Application of Nanosilica for inhibition of fines migration during low salinity water injection: Experimental study, mechanistic understanding, and model development, *Fuel* **242**, 846–862.

Moghadasi R., Rostami A., Tatar A., Hemmati-Sarapardeh A. (2019b) An experimental study of Nanosilica application in reducing calcium sulfate scale at high temperatures during high and low salinity water injection, *J. Petrol. Sci. Eng.* **179**, 7–18.

Mullin J.W. (2001) *Crystallization*, 4th edn., Butterworth-Heinemann, Woburn.

Neff J., Sauer T.C. (1995) *Barium in produced water: Fate and effects in the marine environment*, American Petroleum Institute Publication 4633.

Pingitore N.E. (1987) Modes of co-precipitation of Ba^{2+} and Sr^{2+} with calcite, in: J.A. Davis, K.F. Hayes (eds), *Geochemical processes at mineral surfaces*, American Chemical Society, pp. 574–586.

Pitzer K.S. (1991) *Activity coefficients in electrolyte solutions*, 2nd edn., CRC Press.

Reeder R.J., Lamble G.M., Northrup P. (1999) XAFS study of the coordination and local relaxation around Co^{2+}, Zn^{2+}, Pb^{2+}, and Ba^{2+} trace elements in calcite, *Am. Mineral* **84**, 1049–1060.

Rostami A., Shokrollahi A., Shahbazi K., Ghazanfari M.H. (2019) Application of a new approach for modeling the oil field formation damage due to mineral scaling, *Oil Gas Sci. Technol. – Rev. IFP Energies nouvelles* **74**, 62, 1–10.

Safari H., Jamialahmadi M. (2014) Thermodynamics, kinetics, and hydrodynamics of mixed salt precipitation in porous media: Model development and parameter estimation, *Transport Porous Med.* **101**, 477–505.

Saleh M.M., Mahmoud M.G., El-Lateef H.M.A. (2019) Comparative study of synergistic inhibition of mild steel and pure iron by 1-hexadecylpyridinium chloride and bromide ions, *Corros. Sci.* **154**, 70–79.

Sanni O., Bukuaghangin O., Huggan M., Kapur N., Charpentier T., Neville A. (2017) Development of a novel once-through flow visualization technique for kinetic study of bulk and surface scaling, *Rev. Sci. Instrum.* **88**, 103903.

Stumm W., Morgan J.J. (1996) *Aquatic chemistry*, Wiley-Interscience.

Tesoriero A.J., Pankow J.F. (1996) Solid solution partitioning of Sr^{2+}, Ba^{2+}, and Cd^{2+} to calcite, *Geochim. Cosmochim. Acta.* **66**, 1053–1063.

Vazquez O., Fursov I., Mackay E. (2016) Automatic optimization of oilfield scale inhibitor squeeze treatment designs, *J. Petro. Sci. Eng.* **147**, 302–307.

Wang Y., Xu H. (2001) Prediction of trace metal partitioning between minerals and aqueous solutions: a linear free energy correlation approach, *Geochim. Cosmochim. Acta.* **65**, 1529–1543.

Wang Z., Zhao Y., Zhang J., Pan S., Yu J., Sun B. (2018) Flow assurance during deepwater gas well testing: Hydrate blockage prediction and prevention, *J. Petro. Sci. Eng.* **163**, 211–216.

Yoshida Y., Yoshikawa H., Nakanishi T. (2008) Partition coefficients of Ra and Ba in calcite, *Geochem. J.* **42**, 295–304.

Yuan M. (2010) Latest developments in oilfield scale control, in: Amjad Z. (ed), *The science and technology of industrial water treatment*, CRC Press, pp. 135–159.

Zarga Y., Boubaker H.B., Ghaffour N., Elfil H. (2013) Study of calcium carbonate and sulfate co-precipitation, *Chem. Eng. Sci.* **96**, 33–41.

Zhang P., Harris L., Demiroglu M., Gokool A. (2017) Production chemistry: Exposing hidden treasures or generating complications, OTC- 27666, in: *Proceeding of Offshore Technology Conference, Houston, Texas.*

Zhang P., Zhang N., Liu Y., Kan A.T., Tomson M.B. (2018a) Application of a novel tube reactor for investigation of calcium carbonate mineral scale deposition kinetics, *Chem. Eng. Res. Des.* **137**, 113–124.

Zhang Z., Zhang P., Li Z., Kan A.T., Tomson M.B. (2018b) Laboratory evaluation and mechanistic understanding of the impact of ferric species on oilfield scale inhibitor performance, *Energy Fuels* **32**, 8348–8357.

Zhang P., Zhang Z., Zhu J., Kan A.T., Tomson M.B. (2019) Experimental evaluation of common sulfate mineral scale coprecipitation kinetics in oilfield operating conditions, *Energy Fuels* **33**, 6177–6186.

Zuber A., Checoni R.F., Mathew R., Santos J.P.L., Tavares F.W., Castier M. (2013) Thermodynamic properties of 1:1 salt aqueous solutions with the electrolattice equation of state, *Oil Gas Sci. Technology – Rev. IFP Energies nouvelles* **68**, 2, 255–270.